# PINER: Prior-informed Implicit Neural Representation Learning for Test-time Adaptation in Sparse-view CT Reconstruction (Supplementary Materials)


Bowen Song
Stanford University
bowens18@stanford.edu

Liyue Shen*
University of Michigan
liyues@umich.edu

Lei Xing*
Stanford University
lei@stanford.edu



Figure 1. Performance of PINER on a random test sample against different values of the hyperparameter of prior regularization ($\alpha$)

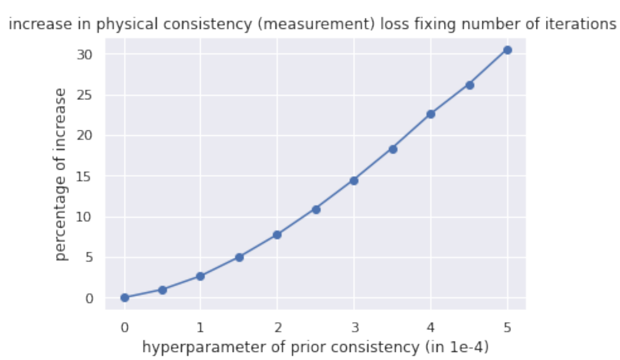


Figure 2. Increase in physical consistency (measurement) loss against different values of the hyperparameter of prior regularization ($\alpha$) with a fixed number of iterations. Here we use the iteration number of the early stopping point when $\alpha = 0$

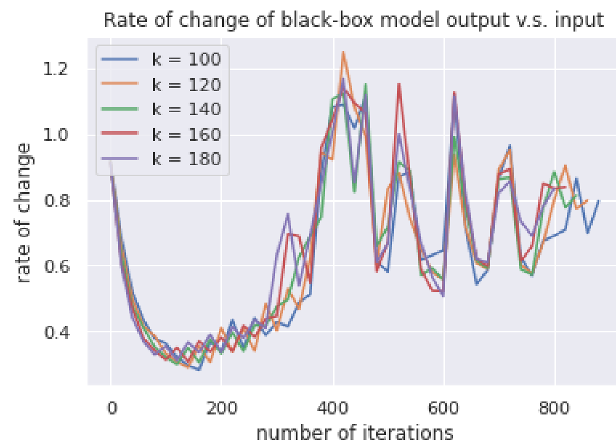


Figure 3. the rate of change $d$ curve for a random test sample for different values of sliding window size $k$ (in number of iterations).

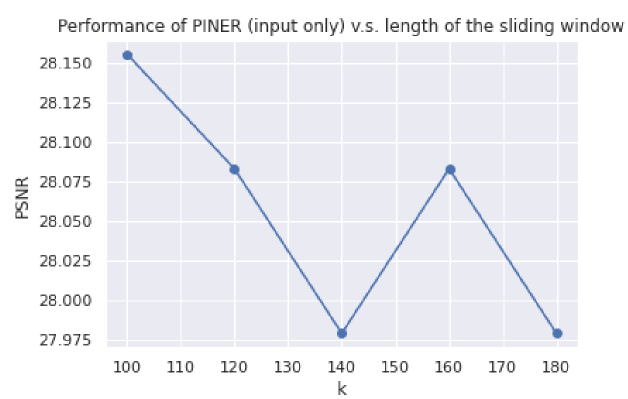


Figure 4. Performance of PINER (input only) on a random test sample v.s. different values of sliding window size ($k$)

## 6. Appendix

### 6.1. Discussion about Hyperparameter Sensitivity

**Prior consistency** ($\alpha$). We conduct experiments in Sec.4 by comparing the performance of PINER (no-reg) with other variants. **We observe that there is only marginal improvement ($< 0.2db$) in performance by adding the prior-consistency term compared to PINER (no-reg).** This observation also implies that the implicit neural representation network [2] may contain internal prior knowledge or implicit regularization so that it can find a good-quality reconstruction by early stopping without any external regularization given a noisy measurement. The performance of PINER (no-reg) on LDCT dataset demonstrated in Table. 1 of this Appendix further solidifies this finding. We conduct further experiments by altering the magnitude of this term. Fig. 1 demonstrates that the performance changes little when altering the magnitude of $\alpha$. Fig. 2 demonstrates the increase of physical consistency loss against $\alpha$ at the $100th$ iteration for a randomly selected test sample. We observe that when the physical consistency loss increases slightly (less than 30 percent), the reconstruction performance does not change significantly.

**Length of the sliding window** ($k$). In all of our experiments, we take a snapshot of a representation per 20 epochs over the total 1000 epochs for memory efficiency and data privacy concerns. Hence, if $k = 140$, it means that the sliding window contains 7 representation images, which corresponds to a length of 7 in Sec.4. Fig. 3 demonstrates the $d$ curve for a randomly selected test sample under different $k$ values (100,120,140,160,180). We observe that the shape of $d$ curve is invariant to different choices of $k$. All of these curves achieve a minimum early and then increase and oscillate. We also plot the performance of PINER (input only) on different values of $k$ for that specific sample in Fig. 4. We do not observe significant difference in performance for different k values. **These observations imply that the performance of PINER is insensitive to different $k$ values when there are small but observable differences between representation images at the end and the beginning of the sliding window.** Generally speaking, a smaller $k$ captures local changes better, while a larger $k$ captures the overall trend better.

**Learning rates** ($\lambda_1, \lambda_2$). The learning rate $\lambda_2$ for physical-consistency optimization is set to be $1e$-$5$ following the setting in [1]. A much larger learning rate for this step may not be suitable for preserving the embedded prior information. The setting of learning rate $\lambda_1$ for the input-adaptation stage is based on the idea that we would not like to achieve a high fitting accuracy in the early iterations so that we can have a granular collection of representations. We decrease the learning rate until we cannot achieve a PSNR of 40db in the last 100 iterations. For simplicity we set the learning rate to be $5e$-$5$ for LDCT dataset, and $3e$-$5$ for LIDC dataset.

## 6.2. Additional Experimental Results and Figures

We included the results for ablation study on the LDCT dataset (tested on Gaussian noise) and the detailed performance of UNet+ on each organ site of the LDCT dataset (tested on Poisson-Gaussian noise) in Table. 1. We also include the ground truth test-time noise level distribution for "OOD noise detected" and "OOD noise not detected" test

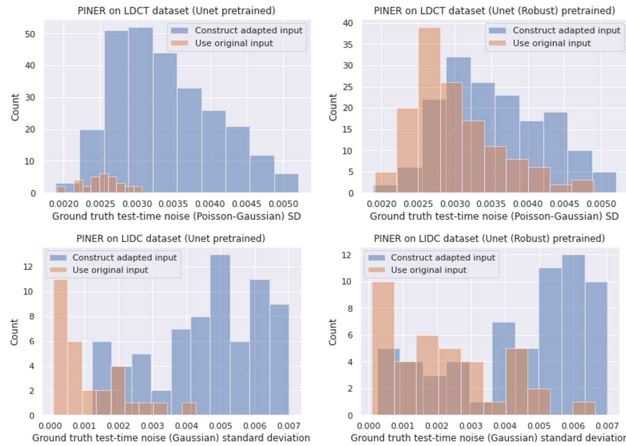


Figure 5. Histograms of ground truth noise distribution for OOD noise detected and OOD noise not detected test-time samples with UNet and UNet+ pretrained. (UNet is trained on noise level 0.0001 and UNet+ is trained on noise levels [0,0.0025])

samples in Fig. 5 for UNet and UNet+ (trained on more noisy data) on both datasets. We observe that in all scenarios, most samples with noise levels in the lower end are not detected as containing OOD noise, and most samples with the noise levels in the higher end are detected as containing OOD noise. We also observe that for UNet+, that distribution is very different from UNet on both datasets, with much more test-time samples with noise level close to the augmented training set for UNet+ not detected as containing OOD noise. All these observations highlight that PINER is able to detect test-time samples that contain OOD noise, and construct an adapted input accordingly.

## 6.3. Visualization of Reconstructions by Different Methods

We provide several additional visualization of reconstruction results on the LDCT dataset and the LIDC dataset in Figs. 6- 9. The critical image structure region is annotated in red and zoomed in. We can find that PINER can reconstruct fine details of images accurately while being a little blurry when the noise level is very high. In contrast, RnR can provide smooth and sharp images, but the details are often inaccurate.

## 6.4. Network Architecture of Implicit Neural Representation

We follow [1]'s approach for the INR network architecture. We construct an 8-layer MLP network with a width of 256 neural nodes f, where each fully-connected layer is followed by the periodic activation function [2] except for the last layer. The Fourier feature embedding [3] size is 256, where the hyperparameter for the embedding scale (standard deviation of the Fourier coefficient's Gaussian distri-

Table 1. Performance of adaptation algorithms on the LDCT dataset with different pretrained models

| Model | Adaptation Method | Abdominal | | Head | | Chest | |
|---|---|---|---|---|---|---|---|
| | | PSNR | SSIM | PSNR | SSIM | PSNR | SSIM |
| UNet | None | 28.67 | 0.799 | 26.58 | 0.707 | 26.68 | 0.771 |
| | PINER (input only) | 29.89 | 0.848 | 27.81 | 0.752 | 28.27 | 0.812 |
| | PINER (physics only) | 32.81 | 0.931 | 32.62 | 0.921 | 29.84 | 0.883 |
| | PINER (no-reg) | 32.97 | 0.933 | 33.01 | 0.925 | 29.92 | 0.870 |
| | PINER (full) | **33.06** | **0.936** | **33.10** | **0.931** | **30.11** | **0.892** |
| DnCNN | None | 29.36 | 0.809 | 29.58 | 0.832 | 28.55 | 0.831 |
| | PINER (input only) | 31.18 | 0.885 | 30.19 | 0.841 | 29.48 | 0.870 |
| | PINER (physics only) | 31.20 | 0.875 | 32.33 | 0.918 | 29.73 | 0.868 |
| | PINER (no-reg) | 34.15 | **0.951** | 34.31 | **0.951** | 31.20 | **0.913** |
| | PINER (full) | **34.22** | 0.948 | **34.40** | 0.947 | **31.30** | 0.912 |
| UNet+ | None | 31.28 | 0.888 | 30.20 | 0.857 | 28.68 | 0.848 |
| | PICCS | 32.35 | 0.927 | 32.15 | 0.924 | 29.42 | 0.877 |
| | RnR | 31.79 | 0.940 | 31.40 | **0.947** | 29.22 | 0.894 |
| | PINER (input only) | 31.60 | 0.899 | 30.28 | 0.859 | 28.93 | 0.862 |
| | PINER (full) | **33.63** | **0.946** | **33.46** | 0.944 | **30.23** | **0.898** |

bution) is set as 4 for CT reconstruction. We use the same network architecture for every experiment.

## References


[1] Liyue Shen, John Pauly, and Lei Xing. Nerp: implicit neural representation learning with prior embedding for sparsely sampled image reconstruction. *IEEE Transactions on Neural Networks and Learning Systems*, 2022.

[2] Vincent Sitzmann, Julien Martel, Alexander Bergman, David Lindell, and Gordon Wetzstein. Implicit neural representations with periodic activation functions. *Advances in Neural Information Processing Systems*, 33:7462–7473, 2020.

[3] Matthew Tancik, Pratul Srinivasan, Ben Mildenhall, Sara Fridovich-Keil, Nithin Raghavan, Utkarsh Singhal, Ravi Ramamoorthi, Jonathan Barron, and Ren Ng. Fourier features let networks learn high frequency functions in low dimensional domains. *Advances in Neural Information Processing Systems*, 33:7537–7547, 2020.

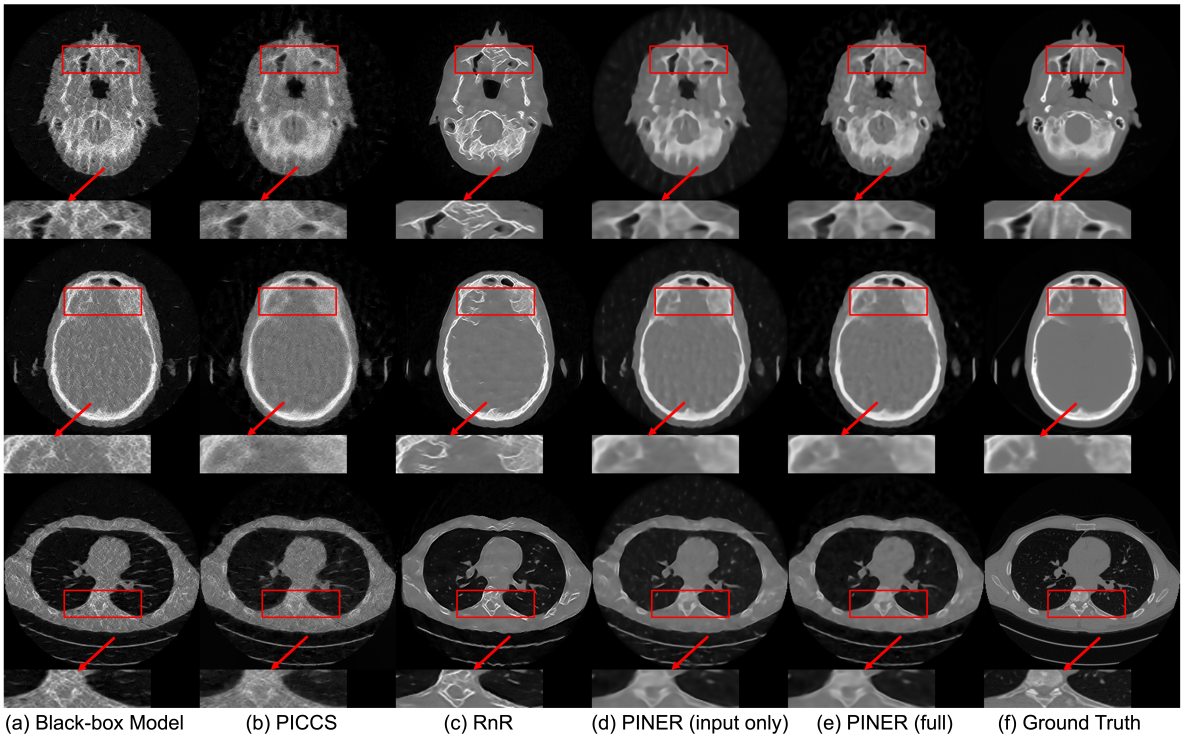


Figure 6. Reconstructions on LDCT dataset

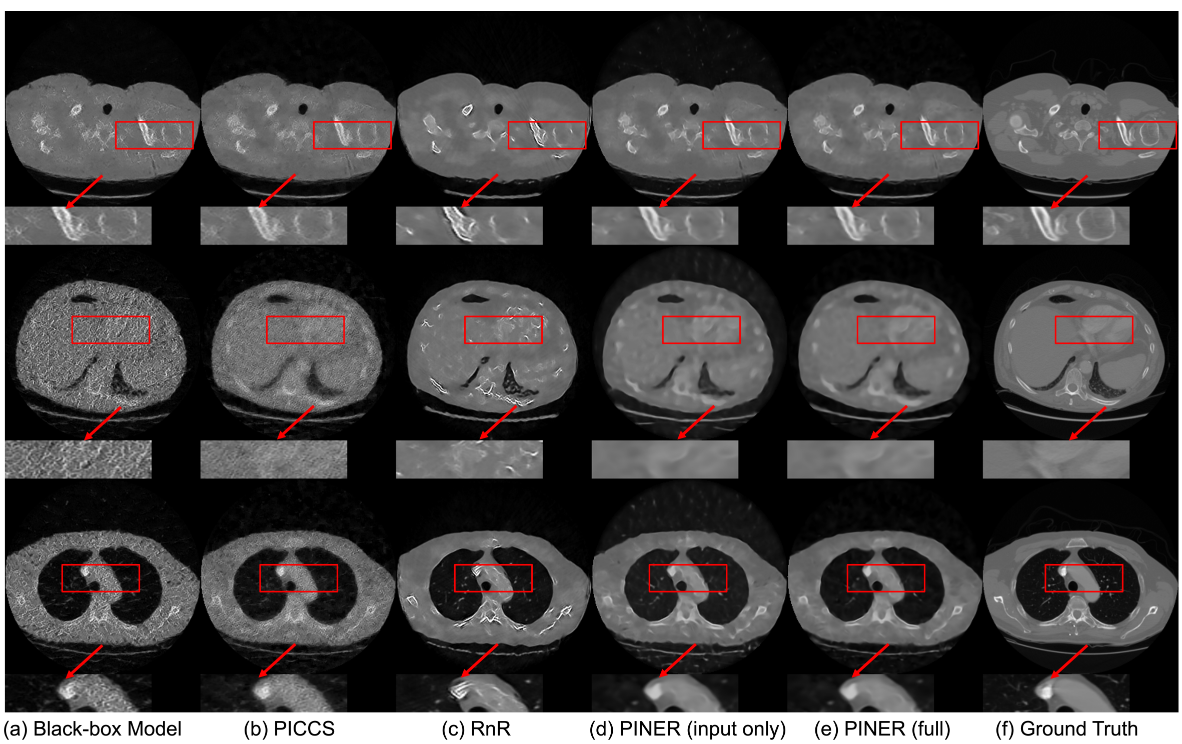


Figure 7. Reconstructions on LIDC dataset

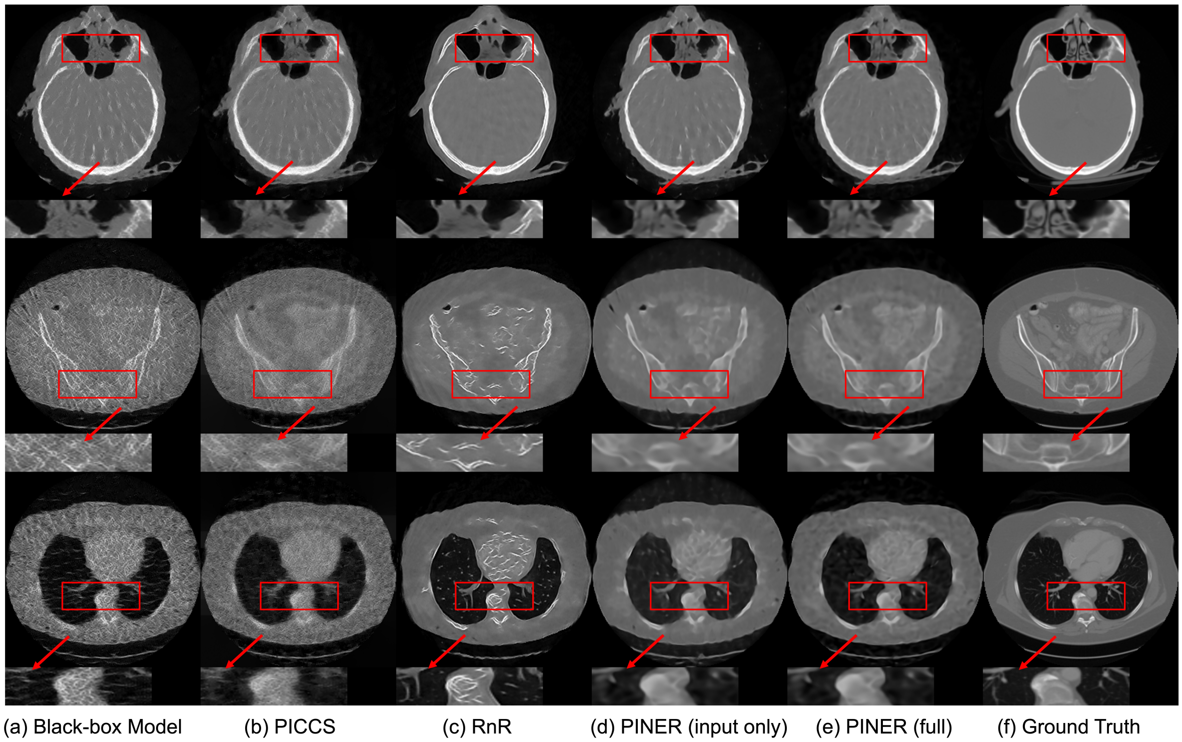


Figure 8. Reconstructions on LDCT dataset

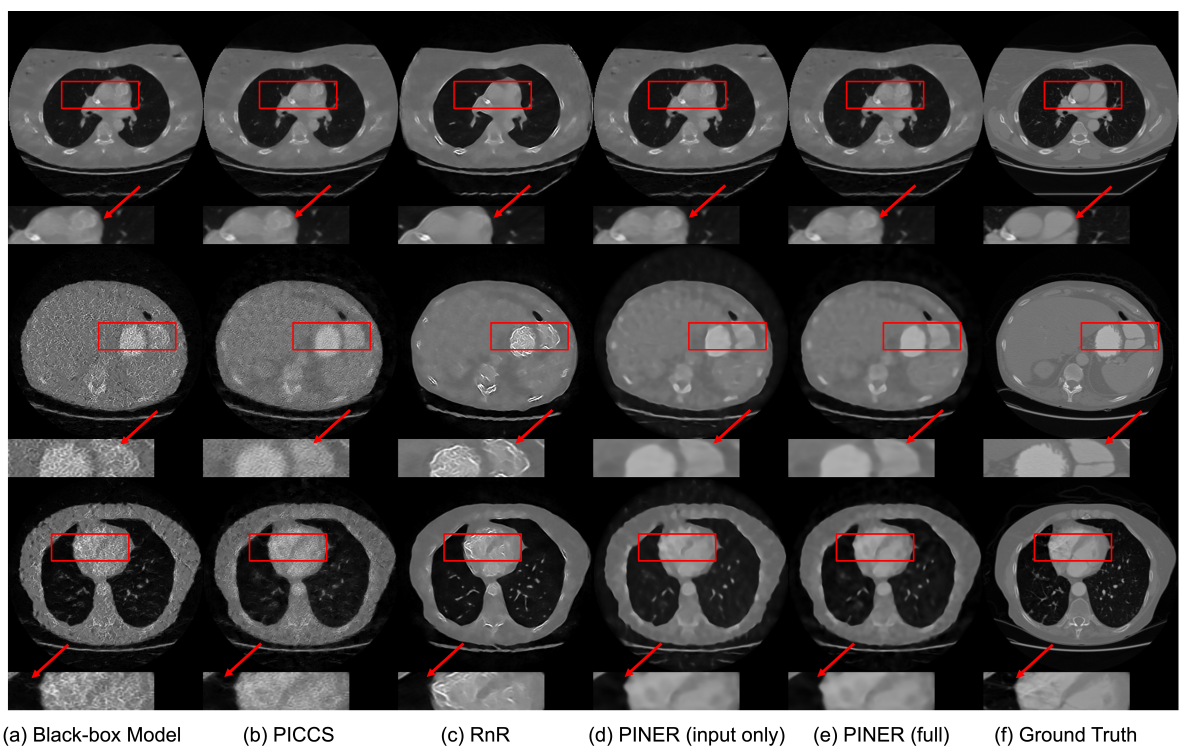


Figure 9. Reconstructions on LIDC dataset